1.5 Strong ground motion recorded during the L'Aquila seismic sequence

F. Pacor[1], R. Paolucci[2], I. Iervolino[3], M. Nicoletti[4], G. Ameri[1], D. Bindi[1], C. Cauzzi[2], E. Chioccarelli[3], E. D'Alema[1], L. Luzi[1], S. Marzorati[1], M. Massa[1], R. Puglia[1] ■

1.5.1 Introduction

Strong motion data during the L'Aquila seismic sequence, started on April 6 2009 at 01:32 am GMT (M_W 6.3), were mainly recorded by the Italian accelerometric network (Rete Accelerometrica Nazionale, RAN), operated by the *Department of Civil Protection* (DPC). Several records were obtained also by a temporary network installed the day after the mainshock by the *Istituto Nazionale di Geofisica e Vulcanologia (INGV MI-PV)*. Data from DPC can be downloaded from the ITalian ACcelerometric Archive ITACA (http://itaca.mi.ingv.it), while data from INGV are accessible from the internet site http://accel.mi.ingv.it/statiche/ABRUZZO-2009/main.html.

The L'Aquila earthquake is the third strongest seismic event producing strong motion records in Italy, after the Irpinia (1980, M_W 6.9) and Friuli (1976, M_W 6.4) earthquakes. This event, together with the 12 strongest aftershocks (M_W > 4.0) provided a unique strong motion dataset in Italy, especially due to the amount and intensity of near-fault records.

The dataset consists of about 300 digital accelerograms (270 of which belonging to RAN), with a very good signal-to-noise ratio, recorded by about 70 stations, installed on different site conditions at distance ranging from 0 to 300 km. The national and international relevance of this dataset is enhanced by its contribution to fill gaps in the magnitude-distance distribution of worldwide strong motion records, especially for normal-fault earthquakes (Ameri et al., 2009).

Near-fault records were obtained by (i) an array of 6 stations installed by DPC in 2001 in the Aterno Valley to study seismic site effects; (ii) station AQK close to downtown L'Aquila; (iii) station AQU, belonging to the broad-band Mednet network (mednet.rm.ingv.it/data.php), located in the L'Aquila historic castle; (iv) the stations of the INGV temporary network, installed in the epicentral region one day after the mainshock. These stations are located less than 5 km distance from the epicenter mainshock, and fall inside the surface projection of the fault rupture.

This work presents an overview of the main features of seismic ground shaking during the L'Aquila sequence, referring to records of the mainshock and of the two strongest aftershocks. The dependence of the strong-motion parameters on distance, azimuth and site conditions is discussed, as well as the effect of near-fault strong motion records on nonlinear structural response.

1.5.2 Characteristics of the accelerometric *data set*

Figure 1 shows the distribution of the strong motion stations recording the L'Aquila seismic sequence and Table 1 lists the main station parameters. The source parameters of the 13 events with $M \geq 4$ analyzed in this study are given in Table 2.

The sites are classified according to the Eurocode 8 (EC8; CEN, 2004) and the Italian Building code (NTC08, 2008), based on the shear-wave velocity averaged over the top 30 m of the soil profile - Vs30 (where EC8 class A > 800 m/s, B = 360-800 m/s, C = 180-360 m/s, and D<180 m/s). In this work, the class of each station has been attributed on the basis of geological/geophysical information (S4 project – http://esse4.mi.ingv.it – Deliverable D4, 2009) and only some stations, for example AQV located in epicentral area, have been classified by a direct measure of Vs30. Most stations belong to class A or B and only a few sites are classified as class C, among them Avezzano and Norcia installed inside alluvial basins. Stations GSA and GSG are located within the *Istituto Nazionale Fisica Nucleare* Laboratory: the former is at ground surface while the latter is in a tunnel inside Gran Sasso mountain at 200 m below the surface and missing GPS signal. The GSG recordings were not used in the following analyses.

[1] INGV - Istituto Nazionale di Geofisica e Vulcanologia, Milano. www.ingv.it
[2] Dipartimento di Ingegneria Strutturale, Politecnico di Milano. www.stru.polimi.it
[3] Dipartimento di Ingegneria Strutturale, Università degli Studi di Napoli Federico II. www.dist.unina.it
[4] Dipartimento della Protezione Civile, Roma. www.protezionecivile.it

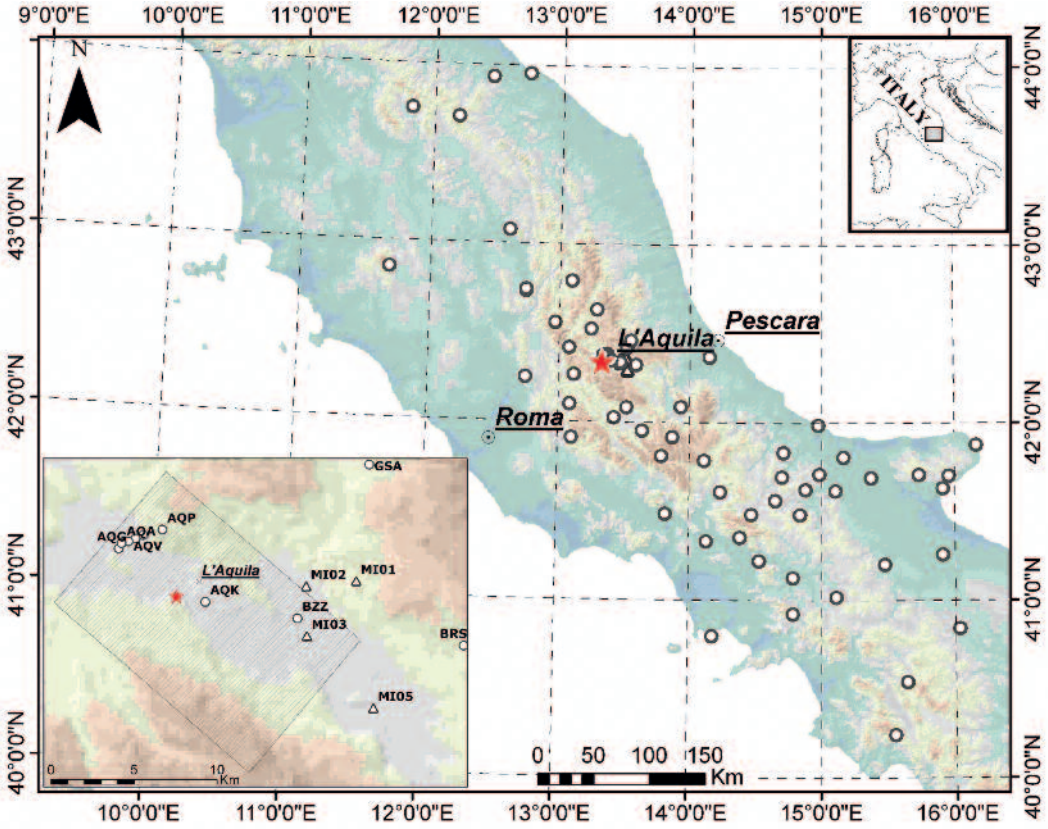

Fig. 1
Location of the accelerometric stations belonging to RAN (circles) and to INGV MI-PV (triangles). The red star denotes the epicenter of the mainshock. In the inset the surface projection of the fault is shown.

The accelerographs installed in the RAN stations are generally Kinemetrics three-component instruments with full scale set to 1 or 2 g, coupled with 24-bit digitizers and sampled at 200 S/s, while the four INGV MI-PV temporary stations were equipped with both an accelerometer (Kinemetrics Episensor ES-T) and a seismometer (either Lennartz 3D-5s or 3DLite) connected to a Reftek130 6 channel digitizer with a sampling rate of 100 S/s.

The strong motion data are available both in the uncorrected and corrected version; the recorded waveforms were processed with the procedure described in Massa et al. (2009). This includes the removal of the linear trend fitting the entire record, a cosine taper and band pass filtering with a time-domain acausal 4th order Butterworth filter. Both the high-pass and low-pass frequencies were selected through visual inspection of the Fourier spectrum. The typical band-pass frequency range is between 0.1 and 25 to 50 Hz; the lower values of the low-cut off frequency have been selected for the stations far away from the epicentre (R_{epi} > 100 km).

Figure 2 shows the distribution of the geometrical mean of Peak Ground Acceleration (PGA)

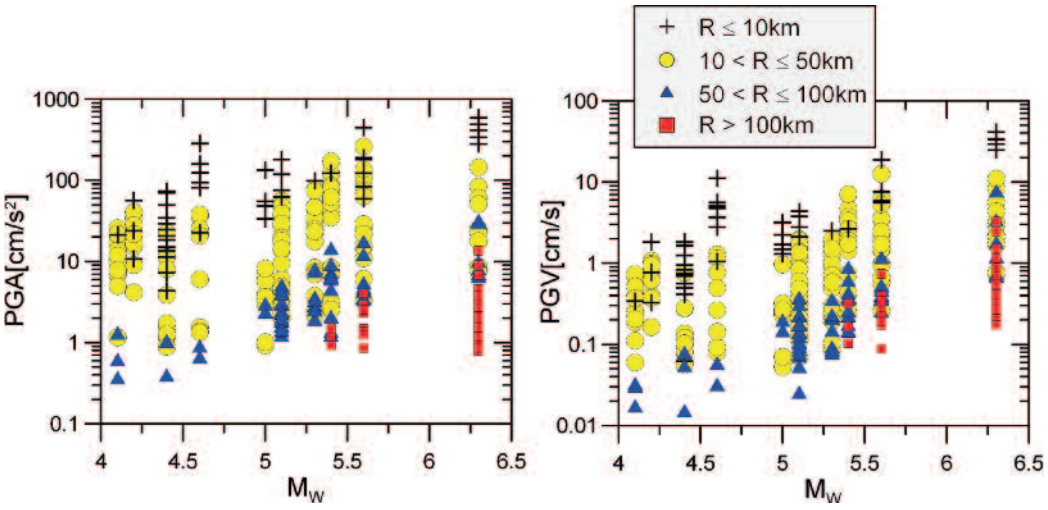

Fig. 2
Geometrical mean between horizontal components of PGA (left) and PGV (right) from the largest earthquakes (M > 4) of the Abruzzo seismic sequence, plotted as a function of Moment-Magnitude. The different symbols indicate different epicentral distance ranges.

and Peak Ground Velocity (PGV), grouped according to epicentral distance ranges, computed from the corrected waveforms, as a function of the moment magnitude.
The largest peak values were recorded in the epicentral area; the maximum PGA and PGV are 0.66 g and 43 cm/s, respectively, recorded at station AQV during the mainshock. The maximum PGA and PGV from the Mw 5.6 event are 0.67 g and 24 cm/s, respectively, recorded at station MI05 (class C) at epicentral distance of 5.3 km. However PGAs larger than 0.2 g were recorded during the 7 April event (21:34 UTC , M_w 4.6) at stations AQM and AQV, located at less than 3 km from the epicenter. It is well-known that PGA shows lower correlation than PGV with respect to magnitude, since PGAs are strongly dependent on the small scale heterogeneities of the wave propagation, causing a weaker dependence on the magnitude event (e.g. Hanks e McGuire, 1981; Faccioli e Paolucci, 2005).

1.5.3 Spatial distribution of ground motion

An overview of the spatial variability of ground motion recorded in the epicentral area during the 6 April earthquake, is illustrated in figure 3 where the maximum horizontal PGA values have been interpolated. In order to better constrain the interpolation, PGA from the stations of the INGV-CNT network were also used. The area of maximum PGA occurs inside the surface projection of the fault, i.e., on the hanging wall. Note that the PGA contours are elongated in the north–south direction.
The attenuation of PGA with distance from the epicenter looks strongly asymmetric, with higher decay rate towards the west. Furthermore, the area corresponding to the 125-300 cm/s^2 PGA range, stretches to the southeast, possibly indicating directivity effects in the rupture propagation along the fault (as also noted by Atzori et al., 2009 e Anzidei et al., 2009).

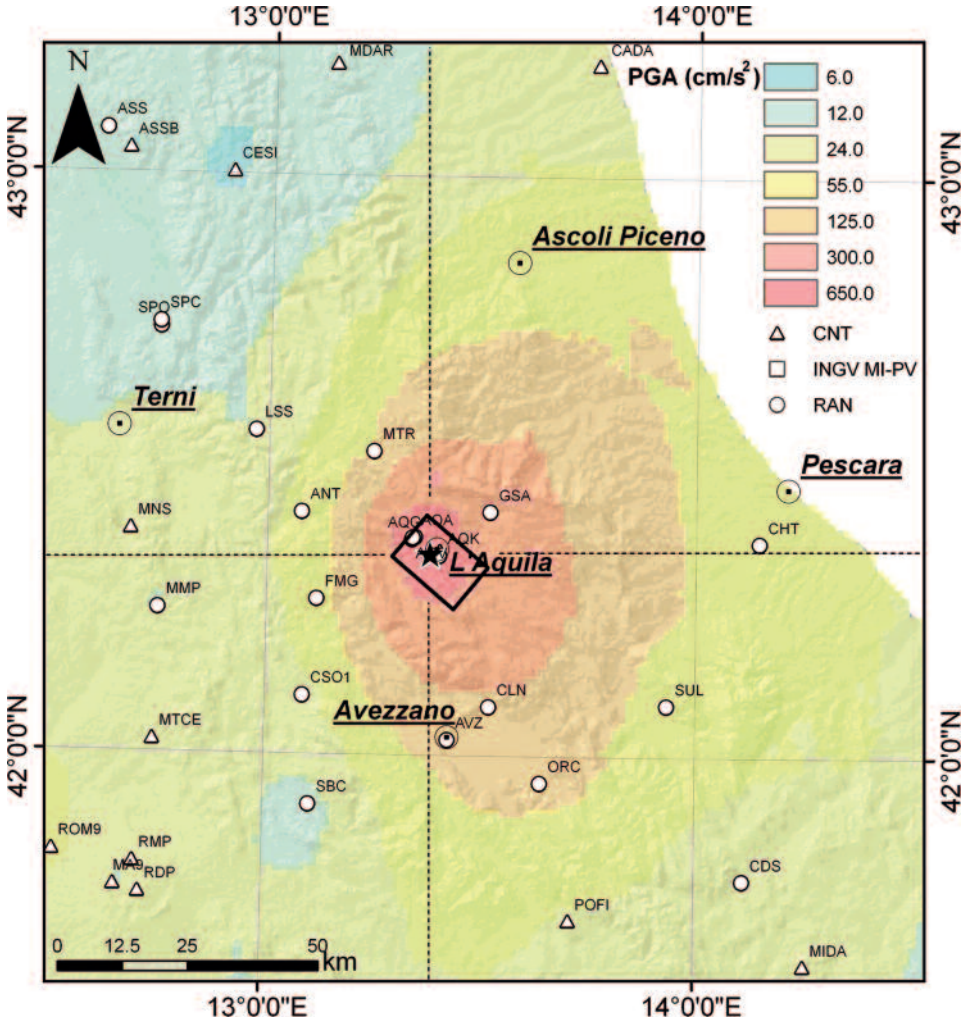

Fig. 3
Peak ground acceleration map (for maximum horizontal component) for the mainshock (modified after Ameri et al., 2009), obtained interpolating data from different seismic networks (triangles: National Seismometric Network, INGV-CNT; dots: Italian Strong-Motion Network, RAN). The star denotes the earthquake epicenter and the black rectangle represents the surface projection of the fault plane. The NE, SE, SW and NW quadrants, with respect to the epicenter, are highlighted.

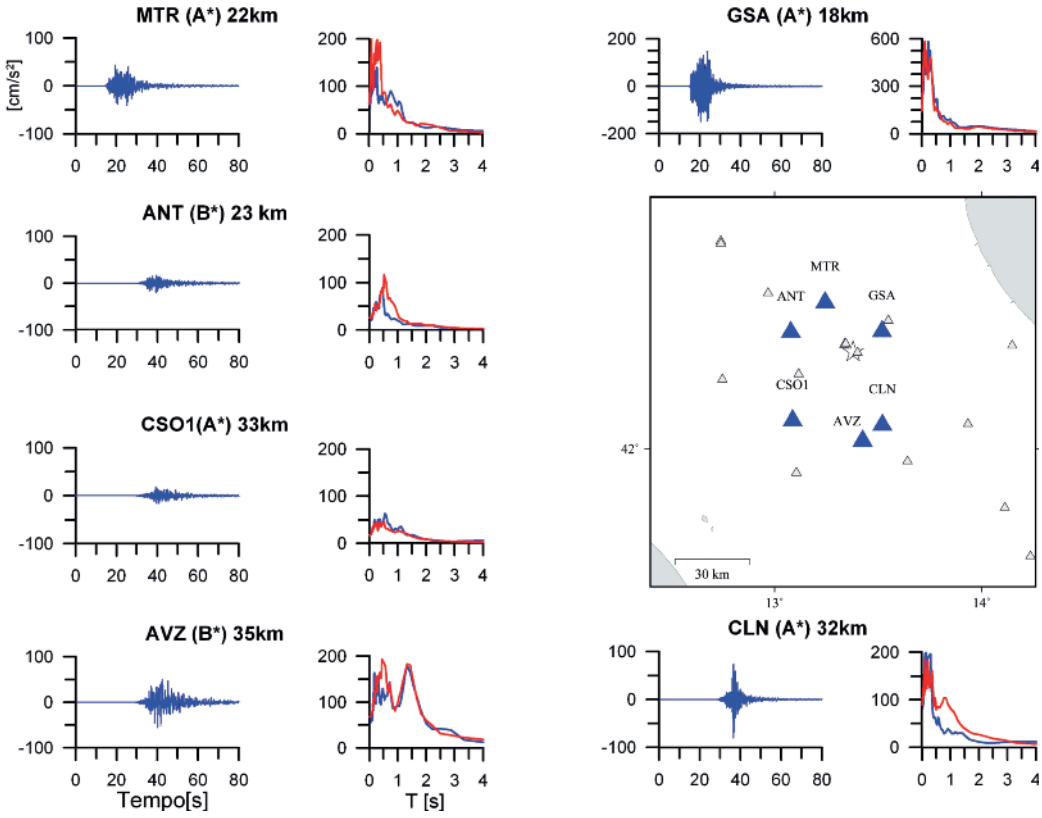

Fig. 4
Acceleration waveforms (EW component) and acceleration response spectra (EW component: blue, NS component: red) recorded during the mainshock by 6 stations (blue triangles). Stations are located in the distance range from 18 to 32 km at difference azimuth with respect to the epicentre (white star). For each station, the code, the site class and the epicentral distance are reported. The white triangles show the position of other accelerometric sites in epicentral area.

The large variability of ground motion in the epicentral area is highlighted in figure 4, where, as an example, the accelerograms (EW component) recorded at 6 stations at 20 to 30 km distance from the epicenter are plotted.
Ground motions recorded at ANT and CSO1 stations, lying West of the epicentre, show lower amplitudes than those at the eastern stations GSA e CLN; furthermore, larger amplitudes are found southward, as shown by the AVZ and MTR recordings, placed in opposite directions with respect to the epicentre. Site effects also play an important role in defining some characteristics of the ground motion. Examples are the large peak at T = 1.5 s of the acceleration response spectra observed at AVZ, together with the high amplitudes of the spectral ordinates in the period range 0 – 0.5 s at GSA.
A more detailed analysis on the azimuth dependence of the seismic ground motions from the L'Aquila earthquakes can be found in Ameri et al. (2009), based on the analysis of the residuals between observed PGA and predicted values by a Ground Motion Prediction Equation (GMPE) calibrated on the Italian strong motion data.

1.5.4 Comparison with the GMPEs

In figure 5 (top panels), the PGAs (mH = maximum between the horizontal components) for the main event, are plotted as a function of the Joyner and Boore distance (R_{JB}, defined as the shortest distance to the surface projection of the rupture surface), and of the soil class.
The grey symbols refer to data located West to the epicentre (azimuth between 180° and 360°) and show systematically lower values than data located in the eastern sectors (0° to 180°), in the distance range 0 – 100 km, confirming the marked directional effects on the ground motion distribution. This asymmetry in attenuation of both PGAs and PGVs suggests that both propagation and directivity effects could have an important role in the interpretation of the ground motion variability in the area.
The data are compared with three recent GMPEs: ITA08 (Bindi et al.; 2009), developed for Italy using the strong motion records available from the ITACA database (http://itaca.mi.ingv.it), AKBO07 (Akkar and Bommer, 2007), based on the European and Middle East data coming from the European strong motion database (http://www.isesd.cv.ic.ac.uk/ESD/); CF08 (Cauzzi and Faccioli, 2008), based on a worldwide database of digital strong motion data, mainly from Japan. In order to compare the results, the original metric of the CF08, correspon-

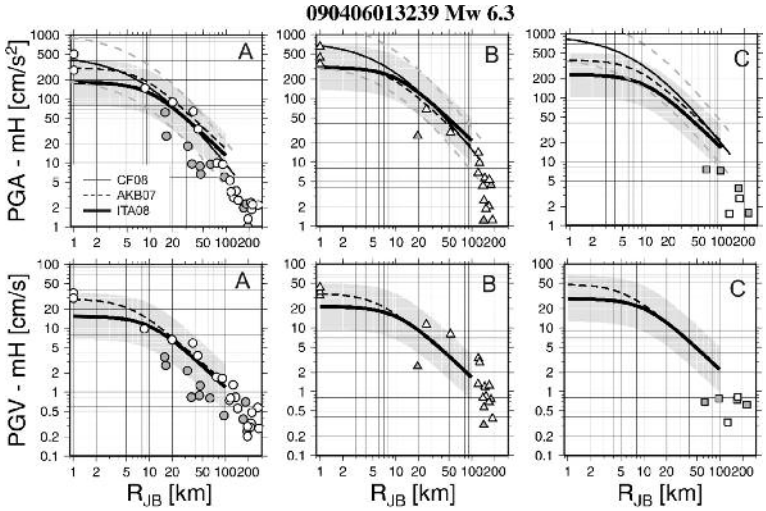

Fig. 5
PGA (top) and PGV (bottom) for maximum horizontal component (mH) versus Joyner and Boore distance (R_{JB}). Data are separated according to EC8 site classification and compared with different ground motion prediction equations. Empty and grey filled symbols correspond to observations over the azimuthal range 0° - 180° and 180° - 360°, computed with respect to the North, respectively (see text for explanation). The shaded area represents the mean plus and minus one standard deviation interval of the ITA08 GMPE. The grey dashed lines represent mean plus and minus one standard deviation of the CF08 GMPE. Note that points with R_{JB} less than 1 km are plotted at 1 km as empty symbols.

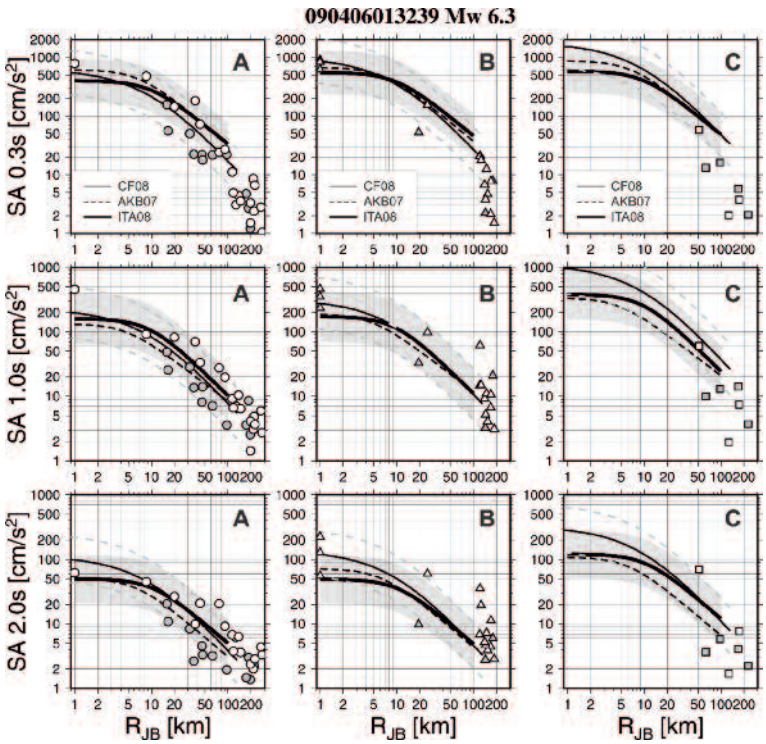

Fig. 6
Spectral acceleration (SA) 5% damped at three reference periods (0.1, 1 and 2 seconds) for maximum horizontal component versus Joyner and Boore distance (R_{JB}) compared with three GMPEs (see text). The same symbols of Figure 5 are used.

ding to the hypocentral distance, has been converted to R_{JB}, through and ad-hoc empirical relation calibrated with the Abruzzo earthquake records, while the geometrical mean between the horizontal components, gM, has been converted to mH (the largest value between the horizontal components) using the relationships proposed by Beyer and Bommer (2006).

On average, the GMPEs fit the data at distances shorter than 150 km, where the empirical models are defined. In particular, the median values of AKBO07 e CF08 equations match reasonably well the near-source data recorded at rock sites On the contrary, ITA08 predicts lower median PGA values, due to the adopted data set that poorly samples the near-fault distances.

Similar considerations can be done regarding the PGVs (Fig. 5, bottom panel) and the spectral ordinates (Fig. 6) at periods 0.3 s, 1.0 s e 2.0 s when compared to the ITA08 and AKO07 predictions.

Figure 7 shows the attenuation of PGAs observed during the strongest aftershock of the sequence (2009/04/07 17:47:37, M_W 5.6) versus the Rjb distance (top panel) and the hypocentral distance (bottom panel) compared with ITA08 and CF08, respectively. Note that we assume Rjb to be equal to the epicentral distance, given the moderate magnitude of the event. In general, a good agreement is found, although the empirical pre-

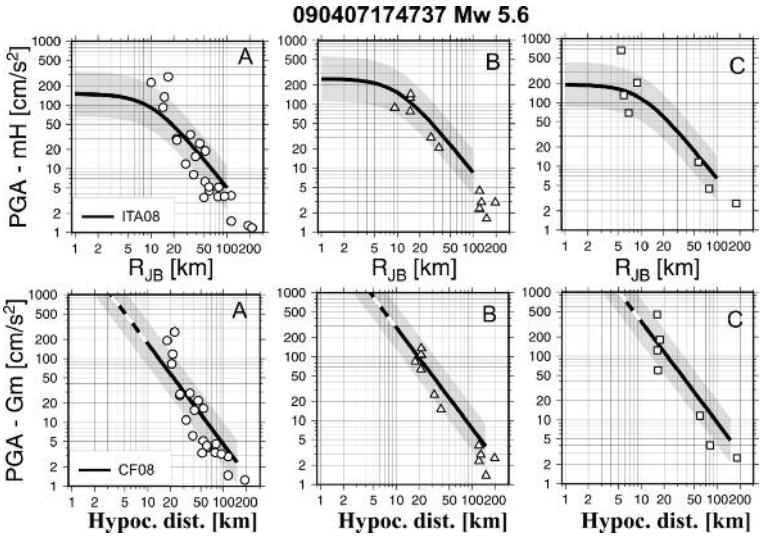

Fig. 7
Maximum horizontal component (top) and geometrical mean, Gm (bottom), of peak ground acceleration from the April 7, Mw 5.6, event versus Joyner-Boore and hypocentral distances, compared with the national GMPE, ITA08 and the global GMPE, CF08, respectively. The shaded area represents the mean plus and minus one standard deviation interval. The CF08 curves are plotted with dashed lines for distances shorter than 10 km, since the model is not constrained by data in this range of distances.

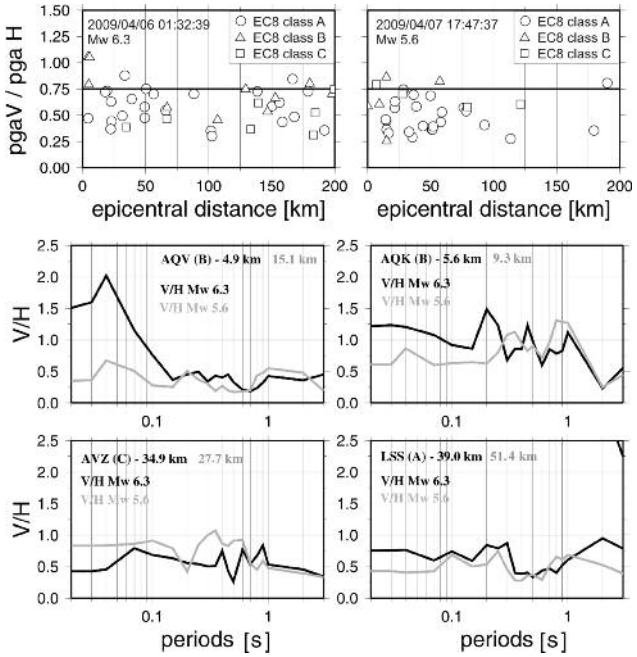

Fig 8
Top: Ratio between vertical and horizontal geometrical mean of PGA versus epicentral distance for the mainshock (left) and the aftershock (right) of the 7 April (17:47). Data are grouped according to the site class. Bottom: Spectral ratio V/H between the vertical and the geometrical mean of the horizontal acceleration response spectra, 5% damped at AQV, AQK, AVZ and LSS, for the mainshock (black line) and the aftershock (grey line) of the 7 April (17:47).

dictions tend to underestimate the observed rock-site PGAs (mH or mG) at distances shorter than about 20 km (ITA08) and 30 km (CF08). A similar pattern, not shown here, is also observed for the second strongest aftershock (2009/04/09 00:52:59, M_W 5.4).

1.5.5 Vertical components of ground motion

Figure 8 (top panel) shows the vertical-to-mean horizontal PGA ratio as a function of distance, both for the mainshock and for the April 7, 17:47, aftershock. Values typically range between 0.25 and 0.75, and the rule-of-thumb of a 2/3 ratio between vertical and horizontal PGA is satisfied on average. Moreover, it is confirmed that, as pointed out several times in the literature (see e.g. Bozorgnia and Campbell, 2004), the peak amplitude of the vertical component may significantly exceed the horizontal one in the near-fault region.

It is also worth noting that the ratio of vertical to horizontal ground motion amplitude may strongly depend on distance and site conditions. For example, in the bottom panels of figure 8 the V/H ratio is shown between the vertical and average horizontal acceleration response spectrum (5% damped) for 4 stations that recorded both the mainshock and the April 7, 17:47, aftershock, located at various distances from the epicenter and for various site conditions.

For the mainshock, the V/H ratios at AQV and

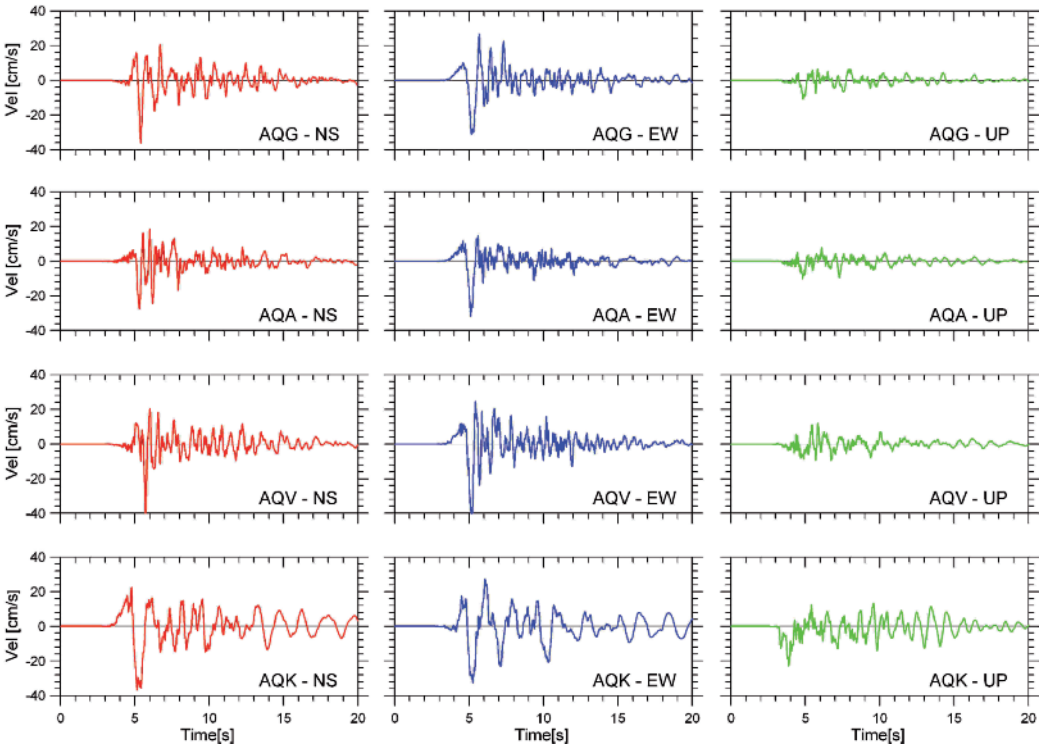

Fig. 9
Velocity waveforms (NS, red, EW, blue and UP, green) at AQG, AQA, AQV and AQK stations for the 6 April earthquake. These stations have the same Joyner-Boore distance.

AQK exceed 1 in the period range 0 – 0.15 s and 0 – 1 s, respectively, while stations located farther away (LSS e AVZ) show values less than unity at all periods.
For the weaker event considered in figure 8, the V/H values lie in the 0.5 – 0.75 range for AQV and LSS stations, while larger values close to 1 in the 0.2 – 1 s range are observed at AVZ and AQK. Although both stations belong to site class B or C, the corresponding vertical records are affected by surface waves arrivals, probably related to complex 2D/3D geological structures.

1.5.6 Near source seismic action and rupture directivity effects

Near-source effects on ground motion have been known for many years both to seismologists and earthquake engineers. The intensity and features of such effects depend on the relative position of the site with respect to the fault rupture, and typically show themselves by large velocity pulses and concentration of energy in the starting phase of the fault-normal components. This results in waveforms different from ordinary ground motions recorded in the far field or in geometrical conditions not favourable with respect to directivity.
Figure 9 shows the velocity time series, recorded during the main event, by three stations in the array of Aterno Valley and by AQK station. In these records the pulse-like features introduced before are visible, especially in the EW components of the first three stations and in both components of AQK station.
Pulse-type records are of interest to structural engineering because they are expected to produce significant difference in terms of structural seismic actions with respect to non-pulse-like records (ordinary in the following), namely: (1) the elastic demand of pulse-like signals is generally stronger than ordinary signals, particularly in the fault-normal direction; (2) the spectral shape is non-standard, showing an increment of spectral ordinates around the pulse period; (3) because the pulse period is generally in the low frequency range (i.e., close to that of the most common structures), the inelastic demand may be particularly high on one side, and, on the other side, it may develop in a shorter time compared to the ordinary case. This may make easier the fragile collapse mechanisms in structures not properly designed.
In the following, the analysis for the assessment of the near fault effects in the main event of L'Aquila earthquakes and the characterization of the corresponding seismic action is briefly described.
Baker (2007) developed a wavelet-based algorithm to identify in the early part of a signal the

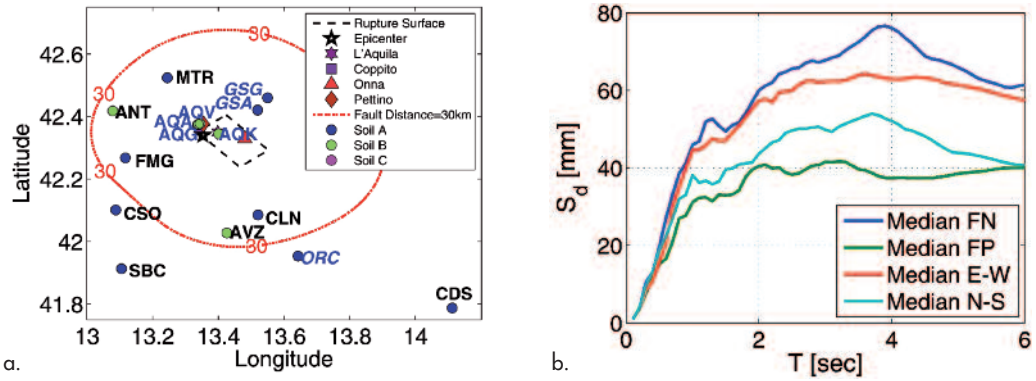

Fig. 10
(a) Map view of rupture surface and RAN accelerometric stations within about 60 km from the fault projection: pulse-like stations are depicted in blue; (b) Median displacement elastic spectra of pulse-like stations in FN, FP, EW and NS directions.

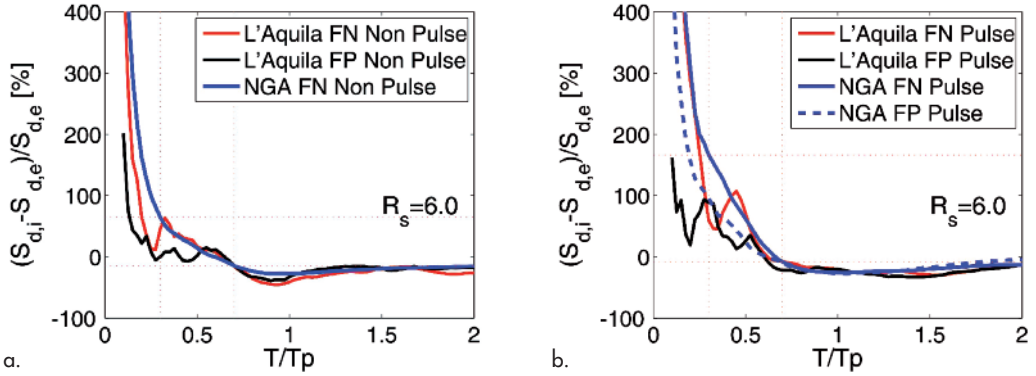

Fig. 11
Inelastic to elastic displacement demand ratio for non-pulse-like (a) and pulse-like (b) stations.

presence or absence of a pulse. The algorithm calculates, for each record, a score from 0 to 1. Records with score above 0.85 and below 0.15 are classified as pulse-like and non-pulse-like respectively, while signals with a score between 0.15 and 0.85 are considered ambiguous. The method was used for the analysis of signals of L'Aquila earthquake recorded by RAN stations. The signals were preliminarily rotated from the original EW and NS directions, to the orthogonal (FN) and parallel (FP) directions with respect to the strike of the fault. This is because the more significant impulsive effects are expected in the FN direction (Somerville et al., 1997).

In particular, thirteen stations having a fault distance lower than 30 km (considered as conventional limit of near-source) were considered. Seven of them have a horizontal component classified as pulse-like: 6 of them in the FN direction and only one in the FP direction (AQV station). The latter one has the FN component as well classified as ambiguous.

Figure 10 shows the projection of rupture surface, the epicentral location, the code of RAN stations (the pulse-like ones are reported in blue) considered in this part of the work, the soil site classification and some severely damaged towns and villages. Moreover, in Table 3 the main characteristics of the considered signals are summarized. For further details about pulse identifications see Chioccarelli and Iervolino (2009a). A similar analysis of the non-rotated records confirms that near-source effects should be studied in FN and FP components. In fact, when the non-rotated signals of the same stations are considered, the identification of pulses in both the NS and EW directions is significantly less coherent. More specifically, 5 signals in EW direction and 4 signals in NS directions were classified as pulses.

Referring to the seven stations with pulse-like signals in FN and FP components, median elastic spectra have been calculated for the four directions considered: fault normal, fault parallel, East-West and North-South. Figures 10b suggests that FN and FP are the directions with higher and lower displacement demand respectively.

In order to analyze pulse-like effects on non-linear structures, several bilinear single degree of freedom (SDoF) elasto-plastic systems with a 3% hardening ratio, a 5% damping ratio and a strength reduction factor Rs = 6 (Rs = ratio between maximum elastic force and yielding force) were considered.

Unexpected displacement demand may occur in structures having non-linear oscillations in a period range around that of the pulse. To illus-

trate this effect, the average inelastic (Sd,i) to elastic (Sd,e) displacement ratios of the bilinear SDoF systems are illustrated in figure 11 for each record as a function of the oscillator period divided by pulse period Tp. Plots are reported for the FN and FP directions of the L'Aquila stations classified as pulse-like and non-pulse-like. They are compared to the same ratios calculated for records of the Next Generation Attenuation (NGA) Project database. Only the NGA FP components of non-pulse-like stations were not plotted as they practically coincide with that of FN non pulse-like.
Referring to NGA records, non-pulse-like stations have a trend that can be considered ordinary and approximately complies with the equal displacement rule. On the contrary, in the case of pulse-like stations (pulse), there is a significant increase of the inelastic displacement for T/Tp between 0.3 and 0.7. In particular, FN components increase by about 170% and -10% respectively in the lower and upper extremes of the period range. This result is a consequence of the peculiar spectral shape of the pulse signals: in fact moving from elastic to inelastic behaviour, SDoF systems have an elongation of the elastic period, which can be twice the one corresponding to the fundamental mode (thus near to the pulse period Tp). The FP components of pulse-like signals have lower increments, but they cannot be considered completely equivalent to non-pulse-like. Although the small sample size, the displacement ratios computed on the L'Aquila records have shapes similar to the NGA results, confirming the importance of near fault effects in the L'Aquila earthquake (Chioccarelli and Iervolino, 2009b).

1.5.7 Conclusions

Due to the quality and amount of data, to their magnitude and distance range and to the variety of site conditions, the seismic sequence of L'Aquila has provided a strong motion dataset of exceptional interest. On one side, the scientific and engineering implications of such data will be relevant to improve the knowledge about seismic ground motion during earthquakes such that of L'Aquila, that are relatively frequent in Italy. On the other side, they will provide the basis for an improved determination of seismic action for design, with special reference to near-fault conditions.
The variability of the peak values of ground motion is consistent with results from the most recent GMPEs. The contour lines of equal peak amplitude tend to elongate towards SE direction, along the same direction as the fault-rupture propagation. Furthermore, the attenuation with distance of ground motion is faster along the west direction, probably related to the different attenuation characteristics towards the Tyrrenian rather than the Adriatic Sea.
Ground motion amplitude in the near-fault region is reasonably well predicted by making use of GMPEs calibrated on a sufficiently large amount of near-fault data. Instead, the use of the Italian strong motion dataset alone, poor in medium-to-large magnitude – short distance records, leads to the underestimation of ground motion amplitude.
In agreement with observations well documented in the literature, peak values of vertical acceleration are close, or even exceed, the corresponding horizontal values in near-fault conditions. At longer distance, the average vertical-to-horizontal PGA ratio tend to approach the value of 2/3. More detailed studies are needed to evaluate the V/H variability as a function of magnitude, distance, site conditions and the implications of such variability in terms of seismic actions for design.
Finally, the effect of the impulsive nature of the seismic motion in near-fault zones for the mainshock of the L' Aquila earthquake was investigated. In particular, the analysis of simple bilinear SDoF elasto-plastic systems shows that the records identified as pulse-like have a peculiar non-linear displacement demand that is compatible with the results expected for signals affected by rupture directivity effects. These results confirm the need of further studies to define the seismic actions in conditions of near-fault, in particular identifying those features of seismic ground motion, in terms of amplitude, duration and frequency content, both useful for a more rational definition of design prescriptions and for a proper evaluation of seismic risk.

Table 1 – Strong motion stations from the RAN (from #1 to #65) and from INGV MI-PV (from #66 to #69), which recorded the L'Aquila seismic sequence. For each station the geographic coordinate, the estimated soil class according to EC8 and the number of records are also shown.

#	Code	Station name	Lat.(N)[°]	Lon. (E) [°]	Site class	#rec
1	AMT	AMATRICE	42.6325	13.2862	A*	1
2	ANT	ANTRODOCO	42.4180	13.0790	B*	12
3	AQA	L'AQUILA - V. Aterno - F. Aterno	42.3760	13.3390	B*	6
4	AQF	L'AQUILA – V. Aterno – Ferriera	42.3805	13.3547	B*	1
5	AQG	L'AQUILA - V. Aterno - Colle Grilli	42.3730	13.3370	A*	10
6	AQK	Aquil PARK ing.	42.3450	13.4010	B*	13
7	AQM	L'AQUILA - V. Aterno – Il Moro	42.3786	13.3493	A*	10
8	AQP	L'AQUILA - V. Aterno – Pettino	42.3837	13.3686	A*	7
9	AQV	L'AQUILA - V. Aterno - Centro Valle	42.3770	13.3440	B	12
10	ASS	ASSISI	43.0750	12.6040	A*	6
11	AVL	AVELLINO	40.9230	14.7870	B*	1
12	AVZ	AVEZZANO	42.0270	13.4260	B*	10
13	BBN	BIBBIENA	43.7480	11.8210	A*	1
14	BDT	BADIA TEDALDA	43.7070	12.1880	A*	2
15	BNE	BENEVENTO	41.1280	14.7850	B*	1
16	BOJ	BOJANO	41.4840	14.4720	B*	4
17	BRS	BARISCIANO	42.3239	13.5903	B*	6
18	BZZ	BAZZANO	42.3370	13.4686	C*	7
19	CAN	CANDELA	41.2030	15.4750	A*	1
20	CDS	CASTEL DI SANGRO	41.7870	14.1120	A*	3
21	CHT	CHIETI	42.3700	14.1480	B	9
22	CLN	CELANO	42.0850	13.5210	A*	7
23	CMB	CAMPOBASSO	41.5630	14.6520	A*	1
24	CMR	CASTELMAURO	41.8330	14.7120	A*	2
25	CNM	CASALNUOVO MONTEROTARO	41.6180	15.1050	B*	1
26	CSO1	CARSOLI 1	42.1000	13.0880	A*	6
27	CSS	CASSINO	41.4860	13.8230	A*	3
28	CTL	CATTOLICA	43.9550	12.7360	B*	2
29	FMG	FIAMIGNANO	42.2680	13.1170	A*	10
30	FOR	FORLI'	44.1990	12.0420	C	1
31	GNL	GENZANO DI LUCANIA	40.8430	16.0330	A*	1
32	GSA	GRAN SASSO (Assergi)	42.4210	13.5190	A*	9
33	GSG	GRAN SASSO (Lab. INFN galleria)	42.4600	13.5500	A*	6
34	ISR	ISERNIA	41.6110	14.2360	C*	1
35	LSS	LEONESSA	42.5580	12.9690	A*	8
36	MMP	MOMPEO 1	42.2490	12.7480	A*	7
37	MNG	MONTE S. ANGELO	41.7040	15.9580	A*	1
38	MNN	MANFREDONIA	41.6340	15.9110	A*	2
39	MTR	MONTEREALE	42.5240	13.2450	A*	10
40	NAP	NAPOLI Ovest	40.7990	14.1800	C*	1
41	NOR	NORCIA	42.7924	13.0924	B*	3
42	ORC	ORTUCCHIO	41.9540	13.6420	A*	11
43	PDM	PIEDIMONTE MATESE	41.3550	14.3850	C*	1
44	PIC	PIANCASTAGNAIO	42.8500	11.6850	B*	2
45	PSC	PESCASSEROLI	41.8120	13.7892	A*	2
46	PTF	PETRELLA TIFERNINA	41.6960	14.7020	B*	3
47	RIC	RICCIA	41.4830	14.8380	B*	1
48	SBC	SUBIACO	41.9130	13.1060	A*	2
49	SCM	S. CROCE DI MAGLIANO	41.7110	14.9840	B*	1
50	SCN	SCANNO	41.9187	13.8724	C*	4
51	SCP	SERRACAPRIOLA	41.8070	15.1650	B*	3
52	SDG	S. GIOVANNI ROTONDO	41.7090	15.7330	A*	1
53	SEP	S. ELIA A PIANISI	41.6250	14.8800	A*	1
54	SNM	SAN MARINO	43.9340	12.4490	A*	2
55	SNS	SANSEPOLCRO	40.2430	15.5500	C*	2
56	SPC	SPOLETO (cantina)	42.7430	12.7400	C*	7
57	SPO	SPOLETO	42.7340	12.7410	A*	7
58	SSR	S. SEVERO	41.6910	15.3740	B	1
59	STL	SATRIANO DI LUCANIA	40.5410	15.6420	A*	1
60	STN	STURNO	41.0180	15.1120	A*	1
61	SUL	SULMONA	42.0890	13.9340	A*	7
62	TLS	TELESE TERME	41.2220	14.5300	A*	1
63	TMO	TERMOLI	41.9890	14.9750	B*	3
64	VIE	VIESTE	41.8770	16.1650	A*	1
65	VRP	VAIRANO PATENORA	41.3330	14.1320	A*	1
66	MI02	PAGANICA	42.3544	13.4745	C*	12
67	MI01	PESCOMAGGIORE	42.3577	13.5109	A*	12
68	MI03	ONNA	42.3274	13.4757	C*	11
69	MI05	S. EUSANIO FORCONESE	42.2890	13.5251	C*	12

*EC8 soil classes estimated according to the available geological/geophysical information (Project S4, http://esse4.mi.ingv.it)

Table 2 – Epicenter coordinates (Lat., Lon.), Depth (H,) Local magnitude, (Ml), Moment magnitude (Mw), strike, dip and rake of the 13 events of the L'Aquila sequence considered in this work

*Date** *yyyymmdd*	hour hour (UTC)* *hhmmss*	*Lat.(N)** [°]	*Lat.(E)** [°]	*H** [km]	*Ml**	*Mw+*	*Strike+* [°]	*Dip+* [°]	*Rake+* [°]
20090406	013240	42.348	13.380	9.5	5.8	6.3	147.0	43.0	-88.0
20090406	023704	42.366	13.340	10.1	4.6	5.1	124.0	62.0	-118.0
20090406	163809	42.362	13.333	10.2	4.0	4.4	143.0	50.0	-123.0
20090406	231537	42.451	13.364	8.6	4.8	5.1	133.0	53.0	-108.0
20090407	092628	42.342	13.338	10.2	4.7	5.0	137.0	56.0	-99.0
20090407	174737	42.275	13.464	15.1	5.3	5.6	109.0	51.0	-124.0
20090407	213429	42.380	13.376	7.4	4.2	4.6	112.0	51.0	-103.0
20090408	225650	42.507	13.364	10.2	4.3	4.1	136.0	71.0	-102.0
20090409	005259	42.484	13.343	15.4	5.1	5.4	148.0	40.0	-90.0
20090409	031452	42.338	13.437	18.0	4.2	4.4	326.0	66.0	-29.0
20090409	043244	42.445	13.420	8.1	4.0	4.2	127.0	62.0	-139.0
20090409	193816	42.501	13.356	17.2	4.9	5.3	146.0	43.0	-75.0
20090413	211424	42.504	13.363	7.5	4.9	5.1	133.0	59.0	-116.0

* After INGV-CNT Bulletin; + after RCMT-INGV; mainshock localization is obtained using seismic records of national local and temporary networks. (INGV, 2009).

Table 3 – Classification of pulse and non-pulse signals, with PGV [cm/sec] and estimated pulse period Tp [s]

	Stations	AQV	AQG	AQA	AQK	GSA	CLN	AVZ	MTR	GSG	FMG	ANT	CSO	ORC
FN	PGV	37.6	**34.1**	**28.7**	**45.0**	**10.9**	5.5	13.1	4.1	**3.7**	2.1	2.3	2.2	**6.7**
	Pulse-like	NO	**YES**	**YES**	**YES**	**YES**	NO	NO	NO	**YES**	NO	NO	NO	**YES**
	Tp	0.5	**1.0**	**0.74**	**2.0**	**3.1**	5.2	1.9	2.6	**4.0**	4.0	1.0	4.8	**0.8**
FP	PGV	**31.4**	26.6	19.9	16.7	6.0	5.8	9.9	3.0	2.3	1.9	2.0	1.5	2.9
	Pulse-like	**YES**	NO	NO	NO	NO	NO	NO	NO	NO	NO	NO	NO	NO
	Tp	**1.1**	1.1	0.6	1.3	2.0	4.8	1.6	2.2	5.2	4.8	2.8	2.2	4.5

Acknowledgements

In this work we made substantial use of the strong motion records of the Italian Accelerometric Network (RAN), operated and maintained by the Italian Department of Civil Protection, – Servizio Monitoraggio del Territorio e Gestione Banche Dati - Ufficio Valutazione, Prevenzione e Mitigazione del Rischio Sismico. The activity of maintenance and update of the Italian strong motion database ITACA (http://itaca.mi.ingv.it) are funded by DPC within Project S4, DPC-INGV agreement 2007-09. Part of the work presented in this paper (Chapter 6) was carried out with the research activity of Consorzio ReLUIS - Rete dei Laboratori Universitari di Ingegneria Sismica (http://www.reluis.it/).

References

Akkar S., Bommer J.J. (2007a) - Empirical prediction equations for peak ground velocity derived from strong-motion records from Europe and the Middle East, *Bull. Seism. Soc. Am.*, 97 (2), 511-530.

Akkar S., Bommer J.J. (2007b) - Prediction of elestic displacement response spectra in Europe and the Middle East, *Earthquake Eng. and Struc. Dyn.*, 36, 1275-1301.

Ameri A., Massa M., Bindi D., D'Alema E., Gorini A., Luzi L., Marzorati S., Pacor F., Paolucci R., Puglia R., Smerzini C. (2009) - The 6 April 2009, Mw 6.3, L'Aquila (Central Italy) earthquake: strong-motion observations, *Seismol. Res. Letters, 80,6, 951-966.*

Anzidei M., Boschi E., Cannelli V., Devoti R., Esposito A., Galvani A., Melini D., Pietrantonio G., Riguzzi F., Sepe V., Serpelloni E. (2009) - Coseismic deformation of the destructive April 6, 2009 L'Aquila earthquake (central Italy) from GPS data, Geophys. Res. Lett. (in stampa).

Atzori S., Hunstad I., Chini M., Salvi S., Tolomei C., Bignami C., Stramondo S., Trasatti E., Antonioli A., Boschi E. (2009) - Finite fault inversion of DInSAR coseismic displacement of the 2009 L'Aquila earthquake (central Italy), Geophys. Res. Lett., 36, L15305, doi:10.1029/2009GL039293.

Baker J.W. (2007) - Quantitative Classification of Near-Fault Ground Motions Using Wavelet Analysis, Bulletin of Seismological Society of America, 97: 1486-1501.

Bindi D., Luzi L., Massa M., Pacor F. (2009) - Horizontal and vertical ground motion prediction equations derived from the Italian Accelerometric Archive (ITACA), *Bull. Of Earth. Eng.*, published on-line. DOI: 10.1007/s10518-009-9130-9.

Bozorgnia Y., Campbell K.W. (2004) - The Vertical-to-Horizontal Spectral Ratio and tentative Procedures for Developing Simplified V/H and Vertical Design Spectra, Journal of Earthquake Engineering, 8 (2): 175-207.

Cauzzi C., Faccioli E. (2008) - Broadband (0.05 to 20s) prediction of displacement response spectra based on worldwide digital records, *J.Seismol.*, 12(4): 453-475.

CEN (2004) - Eurocode 8: Design of structures for

earthquake resistance - Part 1: General rules, seismic actions and rules for buildings, Comité Européen de Normalisation Brussels, May.

Chioccarelli E., Iervolino I. (2009a) - Direttività ed azione sismica: discussione per l'evento de L'Aquila, Proc. of XIII Convegno ANIDIS 2009 "L'Ingegneria Sismica in Italia", Bologna, Italia.

Chioccarelli E., Iervolino I. (2009b) - Near-Source Seismic Demand and Pulse-Like Records: a Discussion for L'Aquila Earthquake, Earthquake Engineering and Structural Dynamics (in press).

Faccioli E., Paolucci R. (2005) - Elementi di Sismologia applicata all'Ingegneria. Pitagora ed.

Hanks T.C., McGuire R.K. (1981) - The character of high-frequency strong ground motion, *Bull. Seismol. Soc. Am.* 71, 2071-2095.

Luzi L., Hailemikael S., Bindi D., Pacor F., Mele F., Sabetta F. (2008) - ITACA (Italian Accelerometric Archive): a web portal for the dissemination of Italian strong-motion data, *Seismol. Res. Letters,* 79, 716-722.

Massa M., Pacor F., Luzi L., Bindi D., Milana G., Sabetta F., Gorini A., Marcocci C. (2009) - The Italian Accelerometric Archive (ITACA): processing of strong motion data, in pubblicazione in *Bull. of Earth. Eng.*

S4 project - Deliverable D4 (2009) - Progress report on the ongoing activity for constructing a catalogue of geological/geotechnical information at accelerometric stations. Available from http://esse4.mi.ingv.it/

Somerville P.G., Smith N.F., Graves R.W., Abrahamson N.A. (1997) - Modification of Empirical Strong Motion Attenuation Relations to Include the Amplitude and Duration Effect of Rupture Directivity, Seismological Research Letters, 68: 199-122.008-9098y.